Arch. Metall. Mater. **71** (2026), 2, 575-578

DOI: https://doi.org/10.24425/amm.2026.158844

SEONG-HO HA[1], YOUNG-CHUL SHIN[1*], SUNG-HWAN LIM[2]

MICROSTRUCTURAL CHARACTERIZATION OF A Cr–Mo–W–Co HOT-WORK DIE STEEL AFTER TEMPERING

The microstructural characteristics of a Cr–Mo–W–Co hot-work die steel subjected to tempering were systematically investigated using scanning electron microscopy (SEM), electron backscatter diffraction (EBSD), and transmission electron microscopy (TEM). All analyses were conducted under a unified tempering condition of 580°C for 6 h in order to establish a coherent interpretation of the stabilized microstructural state. SEM observations revealed the presence of micrometer-scale bright particles whose size and distribution remained unchanged after tempering, indicating that they are pre-existing carbides rather than tempering-induced precipitates. EBSD analysis showed a pronounced change in local crystallographic substructure after tempering, as evidenced by an increase in kernel average misorientation, suggesting sub-grain scale rearrangement within the matrix. TEM and selected area electron diffraction confirmed the formation of crystalline precipitates with well-defined interfaces, which could not be resolved by SEM. STEM-EDS analysis further demonstrated that these precipitates are Mo–W-rich complex alloy carbides incorporating multiple alloying elements.

Keywords: Hot-work die steel; Tempering; Precipitates; Electron microscopy; Microstructural stability

1. Introduction

Hot-work die steels are widely used for tooling in high-temperature metal forming processes such as forging, extrusion, and die casting, where materials are subjected to repeated thermal cycling and severe mechanical loading. To ensure reliable performance, these steels are required to exhibit high thermal stability, resistance to softening, wear resistance, and adequate toughness after heat treatment. Consequently, alloy design and microstructural control have been recognized as key factors governing the service life of hot-work die steels [1,2]. Previous studies have reported that the performance of hot-work die steels is strongly influenced by the stability and evolution of carbides formed during heat treatment. Reviews on hot-work die steels have emphasized that carbide type, size, and distribution play a critical role in resistance to thermal fatigue and high-temperature degradation [1]. In particular, Cr-based hot-work die steels alloyed with elements such as Mo, W, and V have been extensively studied, as these elements contribute to strengthening through carbide formation and solid-solution effects [2].

Recent research has further explored composition-microstructure relationships in hot-work die steels. Chang et al. investigated a hot-work die steel developed through combined compositional design and microstructural refinement, focusing on strength and toughness enhancement via fine precipitates and tempered martensitic structures [3]. Another study proposed a novel martensitic steel containing Ni, Mo, W, and V for hot-work die applications, highlighting the effectiveness of multi-element alloying strategies compared with conventional grades [4]. Di et al. developed a high-toughness 5% Cr hot-work die steel and demonstrated improved thermal stability and thermal fatigue resistance, attributing these improvements partly to changes in carbide distribution and evolution during thermal exposure [5].

Although previous studies have provided valuable insights into carbide evolution in hot-work die steels, most have focused on systems dominated by a single alloying element or carbide type. In contrast, the present study investigates a Cr–Mo–W-based die steel designed with a balanced Mo–W alloying strategy, enabling the formation of chemically complex carbides. This work provides an integrated multi-scale characterization combining SEM, EBSD, TEM, and STEM–EDS under a unified tempering condition, with particular emphasis on correlating sub-grain scale crystallographic evolution with the formation of Mo–W-rich complex carbides. Such an approach offers new insights into the stabilized precipitate–matrix system in Mo–W alloyed hot-work die steels.

[1] KOREA INSTITUTE OF INDUSTRIAL TECHNOLOGY (KITECH), INCHEON 21999, REPUBLIC OF KOREA
[2] KANGWON NATIONAL UNIVERSITY, DEPARTMENT OF ADVANCED MATERIALS SCIENCE AND ENGINEERING, CHUNCHEON 24341, REPUBLIC OF KOREA

* Corresponding author: ycshin@kitech.re.kr

2. Experimental

The material investigated in this study is a hot-work die steel based on the Cr–Mo–W alloy system. The chemical composition of the steel consists of 0.42 wt.% C, 7.5 wt.% Cr, 2.45 wt.% Mo, 2.45 wt.% W, and 9.5 wt.% Co, with the balance being Fe. Minor alloying elements present in small amounts are not explicitly reported. The alloy was subjected to conventional heat treatment consisting of austenitization, quenching, and subsequent tempering. The tempering condition of 580°C for 6 h was selected based on previous isothermal tempering studies on hot-work die steels [6], which demonstrated that holding times on the order of several hours are required to promote microstructural recovery and carbide precipitation at elevated tempering temperatures. After heat treatment, specimens were prepared for microstructural characterization. Scanning electron microscopy (SEM) was employed to observe the overall microstructure and the distribution of carbides. Prior to SEM observation, samples were mechanically ground, polished, and etched using a standard etchant suitable for Cr-based tool steels. SEM observations were conducted using a field-emission scanning electron microscope to obtain sufficient contrast between the matrix and carbide phases. Electron backscatter diffraction (EBSD) analysis was performed to characterize the matrix microstructure before and after tempering. Inverse pole figure (IPF) maps and kernel average misorientation (KAM) maps were acquired to evaluate grain structure and local lattice distortion associated with heat treatment. Transmission electron microscopy (TEM) combined with energy-dispersive X-ray spectroscopy (EDS) was used to analyze nanoscale precipitates formed during tempering, focusing on precipitate morphology, chemical characteristics, and coarsening behavior.

3. Results and discussion

Fig. 1 shows SEM micrographs of the examined alloy in the as-received condition and after tempering at 580°C for 6 h. In both conditions, a number of bright particles are observed within a relatively dark matrix. These bright particles are sparsely distributed and exhibit sizes ranging from several micrometers to tens of micrometers, with irregular morphologies. After tempering at 580°C for 6 h, the overall distribution, size range, and morphology of the bright particles remain essentially unchanged compared to the as-received condition. No noticeable increase in particle size or change in particle density is observed at the SEM length scale. This indicates that the bright particles are stable under the applied tempering condition.

Fig. 2 presents EBSD results obtained from the examined alloy before and after tempering at 580°C for 6 h. Figs. 2(a) and 2(b) show the image quality (IQ) overlaid inverse pole figure (IPF) map and the corresponding kernel average misorientation (KAM) map of the as-received condition. The IPF map exhibits a heterogeneous orientation distribution with clearly defined regions, while the KAM map shows relatively low local misorientation, with an average KAM value of 0.323. After tempering,

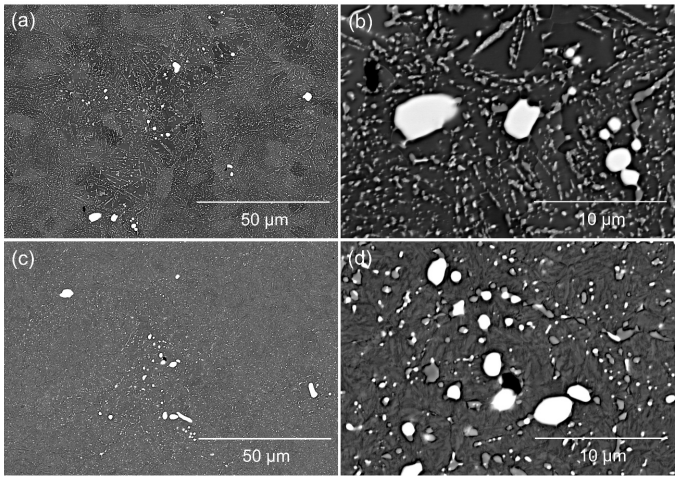

Fig. 1. SEM micrographs of the examined alloy in the as-received condition and after tempering at 580°C for 6 h: (a) as-received condition at low magnification, (b) as-received condition at high magnification, (c) tempered condition at low magnification, and (d) tempered condition at high magnification

the EBSD maps reveal a markedly different microstructural appearance. The IPF map displays a much finer orientation contrast, indicating a fragmented substructure developed during tempering. Correspondingly, the KAM map exhibits a higher level of local misorientation throughout the observed area, with an average KAM value increasing to 0.959. The increase in KAM suggests an increase in local lattice misorientation. Such an increase may be associated with multiple factors, including dislocation rearrangement during recovery as well as local strain fields that can arise during tempering. These results indicate that tempering leads to a significant rearrangement of the crystallographic

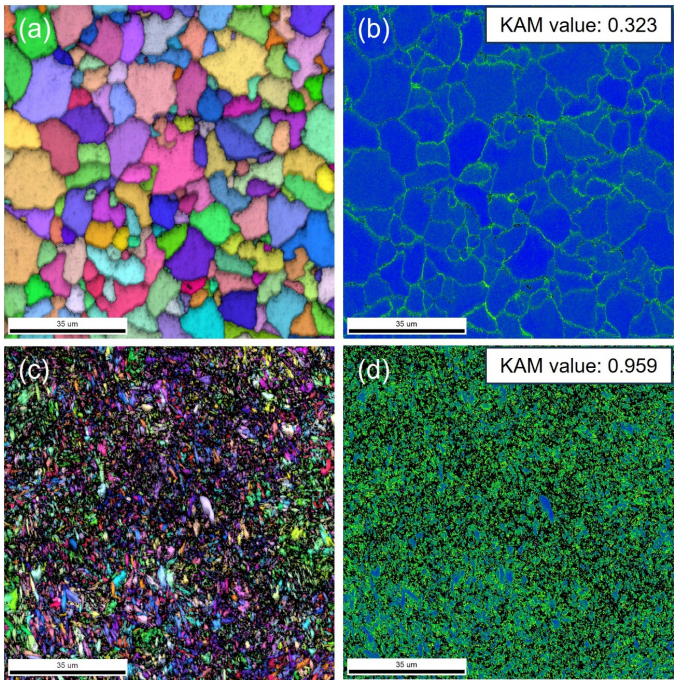

Fig. 2. EBSD maps of the examined alloy: (a) IQ + IPF map and (b) KAM map of the as-received condition, and (c) IQ + IPF map and (d) KAM map after tempering at 580°C for 6 h

substructure, while maintaining overall phase continuity. The EBSD observations demonstrate that microstructural evolution during tempering primarily occurs at the sub-grain scale rather than through changes detectable by SEM.

Fig. 3 shows TEM bright-field (BF) images and the corresponding selected area electron diffraction (SAED) pattern obtained from the alloy tempered at 580°C for 6 h. At low magnification, numerous particles are observed to be dispersed throughout the matrix (see Fig. 3(a)). These particles exhibit a relatively uniform distribution at the submicron scale, while the surrounding matrix shows fine contrast variations. A higher-magnification TEM image reveals an individual particle embedded in the matrix (see Fig. 3(b)). The particle exhibits a faceted morphology with a characteristic size on the order of several tens to hundreds of nanometers. Further magnification highlights a clear contrast between the particle and the surrounding matrix as shown in Fig 3(c), indicating that the particle corresponds to a distinct phase with a well-defined interface. The SAED pattern obtained from the particle shows well-defined diffraction spots rather than diffuse rings, confirming that the particle is crystalline. The diffraction pattern is clearly different from that of the bcc iron matrix, suggesting that the particle corresponds to a crystalline precipitate formed during tempering.

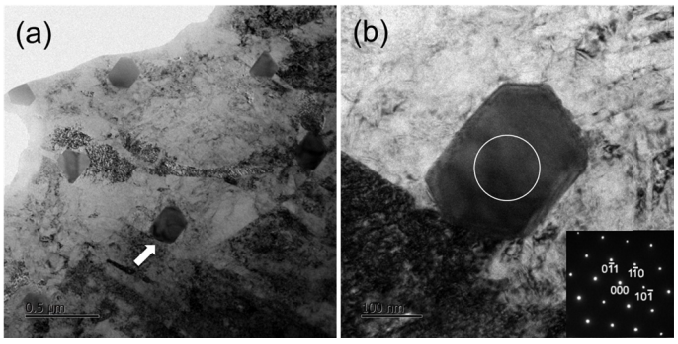

Fig. 3. TEM observations of the alloy tempered at 580°C for 6 h: (a) low-magnification bright-field image showing the distribution of precipitates (indicated by arrows) within the matrix and (b) high-magnification image of an individual precipitate with a well-defined interface, along with the corresponding SAED pattern (inset) indexed to indicate the crystallographic structure of the precipitate

Fig. 4 shows a STEM image and the corresponding EDS elemental maps obtained from the alloy tempered at 580°C for 6 h. The STEM image reveals multiple particles embedded within the matrix at the submicron scale. These particles exhibit a darker contrast relative to the surrounding matrix, consistent with the presence of elements with higher atomic numbers. The EDS maps demonstrate a clear chemical distinction between the particles and the matrix. Iron is uniformly distributed throughout the matrix, whereas tungsten and molybdenum are strongly enriched within the particles. In addition, silicon is also detected in the particles, although at a lower intensity compared to W and Mo. In contrast, chromium and cobalt show relatively uniform distributions and do not exhibit pronounced enrichment within the particles. The combined STEM and EDS results indicate that the observed particles correspond to complex alloy carbides enriched in Mo and W, with additional incorporation of Si. These chemical features are consistent with the formation of thermally stable precipitates during tempering.

By combining STEM imaging with elemental mapping, the present study reveals that the precipitates formed during tempering are not simple binary carbides but Mo–W-rich complex alloy carbides incorporating multiple alloying elements. Based on the enrichment of Mo and W and the observed particle morphology, the precipitates are likely to correspond to M_6C-type carbides, which are commonly reported in Mo–W alloyed hot-work die steels during tempering. However, the possibility of metastable M_2C-type carbides cannot be excluded without detailed crystallographic analysis. The presence of these nanoscale precipitates suggests that precipitation-induced local lattice distortion may contribute to the increased KAM values observed in the EBSD analysis. Importantly, these precipitates coexist with a stabilized matrix structure observed by EBSD and remain distinct from the coarse particles detected by SEM. This integrated observation demonstrates that the examined alloy attains a stabilized microstructural state under the applied tempering condition, characterized by chemically complex and thermally stable precipitates. The formation of Mo–W-rich complex carbides is expected to enhance high-temperature strength and resistance to softening due to their high thermal stability and slow coarsening

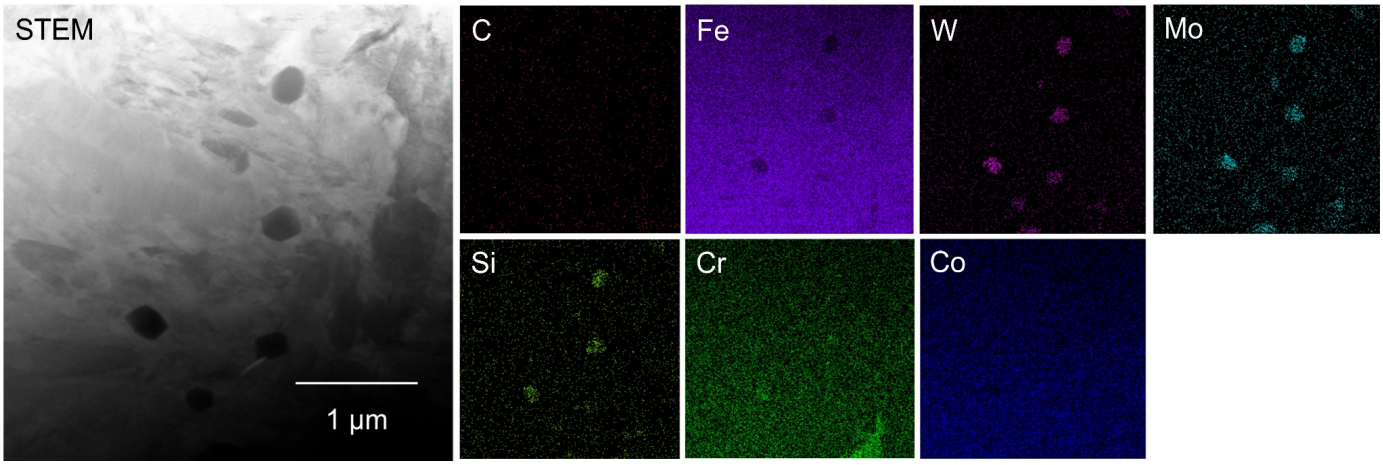

Fig. 4. STEM image and corresponding EDS elemental maps of the alloy tempered at 580°C for 6 h

kinetics. Furthermore, the fine dispersion of these precipitates may contribute to improved resistance to thermal fatigue in hot-work die applications.

4. Conclusions

In this study, the stabilized microstructure of a Cr–Mo–W–Co hot-work die steel tempered at 580°C for 6 h was comprehensively characterized using complementary electron microscopy techniques. SEM observations confirmed that micrometer-scale bright particles are stable and unaffected by tempering, while EBSD revealed significant crystallographic substructure rearrangement within the matrix at the sub-grain scale. TEM observations demonstrated the presence of nanoscale to submicron crystalline precipitates with well-defined interfaces, which were further identified by STEM-EDS as Mo–W-rich complex alloy carbides incorporating multiple alloying elements. By integrating SEM, EBSD, TEM, and STEM-EDS analyses under a unified tempering condition, this work provides a coherent understanding of the stabilized precipitate-matrix system in the examined alloy. The formation of chemically complex and crystalline precipitates under practical tempering conditions offers a microstructural basis for the high-temperature stability required in aluminum forming die applications.

Acknowledgments

This study has been conducted with the support of the National Research Foundation of Korea (NRF) grant funded by the Korea government (MSIT) (No. [RS-2024-00441999]).

REFERENCES

[1] H.-Y. Cui, Z.-J. Bao, Q. Gong, S.-Z. Bao, Y.-Z. Zou, A.-M. Li, H.-Y. Yang, C.-G. Wang, Z.-G. Li, F. Chang, S.-L. Shu, J. Kang, M. Zhu, F. Qiu, Q.-C. Jiang, Materials **17**, 3455 (2024).

[2] W. Gong, J. Yue, J. Tian, J. Liao, Y. Yu, Z. Jiang, J. Mater. Res. Technol. **27**, 4452 (2023).

[3] F. Chang, C.-D. Li, H.-Y. Yang, F. Qiu, S.-L. Shu, L.-Y. Chen, Q.-C. Jiang, J. Mater. Res. Technol. **25**, 1748 (2023).

[4] J. Chen, P. Jin, S. Wang, C. Zhu, M. Xu, Z. Jia, X. Liu, C. Zhao, C. Zhang, J. Huang, Tribol. Int. **207**, 110618 (2025).

[5] Y. Di, D. Ma, H. Chi, J. Gu, B. Fu, J. Zhou, J. Mater. Res. Technol. **33**, 2464 (2024).

[6] H. Wang, H. Feng, H. Li, S. Zhang, H. Zhu, Z. Jiang, Mater. Charact. **212**, 114010 (2024).